V International Scientific and Technical Conference Actual Issues of Power Supply Systems

Development of control components for small-scale wind turbines

AIPCP25-CF-ICAIPSS2025-00560 | Article

PDF auto-generated using **ReView** from

RIVER VALLEY TECHNOLOGIES

Development of control components for small-scale wind turbines

Nikolai Tsybov [1], Zhalalidin Galbaev [1], Samat Umetaliev [1], Buboaisha Bekjanova[1], Eldar Usmanov[2, a]

[1] *Kyrgyz State Technical University N. A. I. Razzakov, Bishkek, Kyrgyz Republic*
[2] *Tashkent state technical university named after Islam Karimov, Tashkent, Uzbekistan*

[a)] *Corresponding author: eldorgu777@gmail.com*

Abstract. Amidst the rapid growth of energy-intensive industrial production and the need to address environmental issues associated with the use of traditional energy sources such as oil, gas, and coal, the global community is paying particular attention to alternative renewable energy sources. Wind energy is one such environmentally friendly source. The objective of this study was to develop control elements and devices for a low-power wind turbine. A *3.5 kW* vertical-axis wind turbine was used as the experimental setup. Through experimental modeling of control modules for the low-power wind turbine, the main control components for the wind turbine (WT) were developed.

INTRODUCTION

The challenging global environmental situation and the depletion of oil, gas, and coal reserves are accelerating the development of renewable energy sources.

According to research into the Kyrgyz Republic's energy sector conducted by Unison Group specialists in 2022, Kyrgyzstan's total hydropower potential is *142.5* billion kWh, ranking third in the CIS. Kyrgyzstan's climatic conditions provide opportunities for solar, wind, hydroelectric, and biomass energy production [1].

Wind energy is one of the promising renewable energy sources in Kyrgyzstan. The latest stage of wind energy development is characterized by renewed interest in small-capacity wind turbines, the market for which has expanded due to the growing number of farms and cottage properties, as well as other hard-to-reach agricultural facilities.

Low-capacity wind energy in Kyrgyzstan is primarily in demand for facilities located in the country's mountainous regions. Kyrgyzstan's mountainous regions are characterized by constantly changing wind directions. For such mountainous regions, low-power wind turbines (WTs) with a vertical axis of rotation, which can operate in any wind direction, are of particular interest [2, 3].

The advantages of vertical wind turbines (WTs) also include the ability to install the turbine equipment closer to the ground, simplifying equipment installation and maintenance [4].

Vertical WTs are more environmentally friendly and generate less noise in high winds. Unlike horizontal-axis wind turbines, vertical WTs do not require wind direction sensing devices, such as additional electric motors and gearboxes for rotor movement. Consequently, WT controllers for vertical WTs do not require complex circuit design [5-8].

A distinctive feature of vertical WTs is the ability to position them much closer to one another, unlike horizontal WTs, which impose strict requirements for the absence of airflow interference during operation.

The most pressing challenges in the design of vertical WTs are the development of WT control systems, as well as the analysis and research of methods for increasing wind turbine performance.

EXPERIMENTAL RESEARCH

Let's consider the control systems for the operating modes of a vertical-axis wind turbine using a *3.5 kW* wind turbine as an example.

The main components of a vertical-axis wind turbine control system are:

– a 3-phase rectifier;

– a charge controller that charges and protects the batteries;

– an inverter that converts the DC voltage of the batteries to AC voltage of *220 V 50 Hz*.

Let's consider the operating features of a low-power wind turbine using a *3.5 kW* vertical-axis wind turbine as an example [9].

Designing a 3-phase rectifier.

When designing a rectifier, Schottky diodes are typically used, which have a low voltage drop across the open *p-n* junction. At a power of *3.5 kW* and a wind turbine output voltage of *24 V*, the output voltage of a rectifier designed using the Larionov design will be *2.34* times higher than *24 V,* or *56 V*. Taking into account the drop across the rectifier diodes, the output voltage will be *54 V*. The average load current will be:

$$I_{AV} = \frac{P}{U} = \frac{3500}{54} = 64,8 \ A$$

In this case, the pulse current required by the charge controller, which will come from the rectifier taking into account the efficiency of the system *(0.8–0.9)* rectifier – controller – inverter will be:

$$I_{PC} = \frac{P}{U \cdot EK} = \frac{3500}{24 \times 0.85} = 171.5 \ A$$

Where I_{PC} – is the rectifier's pulse current, P – is the rectifier's power, U – is the rectifier's output voltage, and EK – is the efficiency of the entire system (rectifier, charge controller, inverter).

Therefore, for a rectifier power of 3.5 *kW,* it is advisable to use *MPRH200200R* Schottky diodes with an on-state current of *200 A* and an allowable reverse voltage of *200 V*.

Designing a charge controller with wind turbine component protection functions.

A battery charge controller (*BCC*) enables battery charging while simultaneously providing the rated load current.

A controller for a low-power *3.5 kW* wind turbine (*WT*) must perform the following functions:

Charging batteries with a current level acceptable for safe charging (*20-30%* of the total battery capacity) [10-12].

Protecting the WT from storm winds of *25 m/sec*.

Protecting the rectifier from unacceptably high output voltage.

Protecting batteries from unacceptable overcharging (up to *28 V*) and unacceptable underdischarging (up to *24.5 V*).

When overcharging batteries or in emergency situations involving storm winds, disconnect the batteries and connect ballast resistors.

It's advisable to base the design of a low-power wind turbine controller on a current stabilizer that regulates a set current using a pulse-width modulator with two negative feedback loops: a charging current feedback loop and a battery voltage feedback loop.

The negative current feedback loop maintains the set battery charging current, while the negative voltage feedback loop controls the maximum permissible battery charging voltage.

The charge controller's circuit diagram is shown in Figure 1.

The charge controller operates as follows:

In the absence of an emergency situation, such as a storm, and therefore no unacceptably high voltage at the output of the three-phase rectifier, a voltage of *30 V* to *95 V* is supplied to the charge controller input, depending on the wind strength.

If the batteries are in charging mode (battery voltage is between *24.5 V* and *27.5 V*), the charge controller charges the batteries with a maximum current of *160 A*.

The charge controller's pulse-width modulation (PWM) signals are generated by the integrated *UC 3842* PWM controller *(pulse-width modulation controller).* The block diagram of the *UC 3842 PWM* controller is shown in Figure 2. The *UC 3842 PWM* controller has two negative feedback inputs.

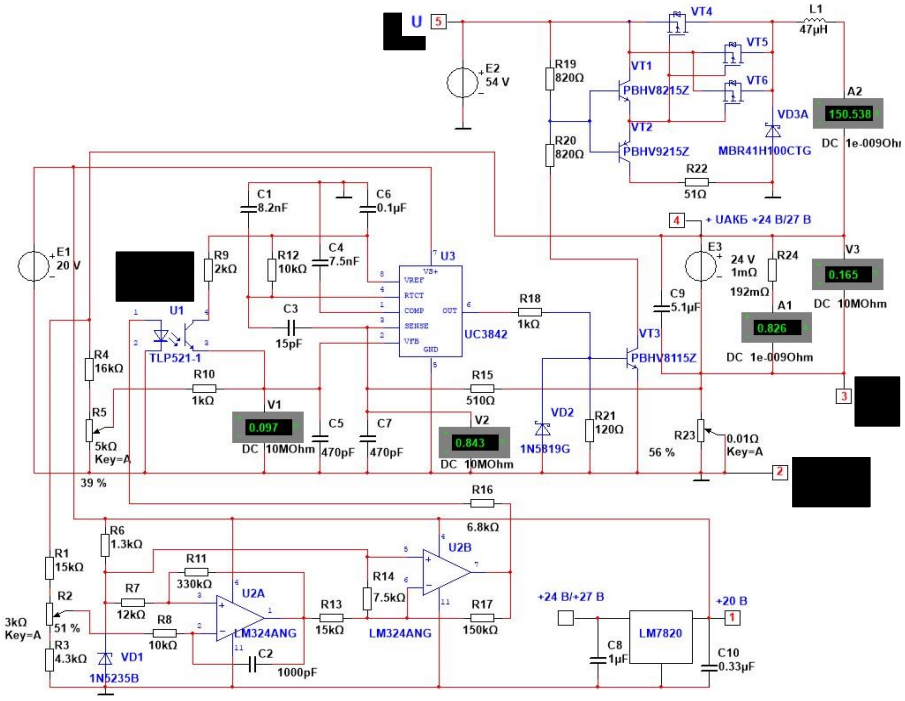

FIGURE 1. Battery charge controller

The negative current feedback signal is fed to input *3* of the *UC 3842 PWM* controller, and the negative voltage feedback signal is fed to input *2* of the *PWM* controller.

Input *2* of the *UC 3842 PWM* controller is the inverting input of the *UC3842* error amplifier, whose non-inverting input is fed a *2.5 V* reference voltage (see Figure 2). Therefore, the error amplifier monitors the negative voltage feedback signal, comparing it to the *2.5 V* threshold voltage.

The negative voltage feedback signal is taken from the positive terminal of the battery and fed through the R_4-R_5 voltage divider and resistor R_{10} to input *2* of the *UC*3842 *PWM* controller. It is then compared with the *2.5 V* voltage supplied to the non-inverting input of the *UC 3842* error amplifier from the reference voltage source.

The charging process occurs at an operating voltage of *24.5 V* to *27.5 V* on the batteries.

The parameters of the wind turbine control system components are calculated as follows.

The charge controller's pulse width modulation frequency is determined by the ratio of capacitor C_1 to resistor R_{12} (see Fig. 1). With a capacitance of *8.2 nF* and a resistor of *10 kOhm*, the pulse width modulation frequency will be *20 kHz*. Capacitors C_4, C_5, *C6,* and C_7 are included in the circuit to ensure noise immunity for the *UC 3842 PWM* controller.

Capacitor C_4 is installed at the output of the error amplifier (pin *1* of the *UC 3842*). The error amplifier current is limited to *1 mA*, and the maximum voltage at its output does not exceed the reference voltage of *5 V*. Therefore, the output impedance of the error amplifier is:

$$R = \frac{U}{I} = \frac{5}{0.001} = 5 \quad k\,Om,$$

Where R – is the error amplifier output resistance; U – is the reference voltage; and I – is the error amplifier current.

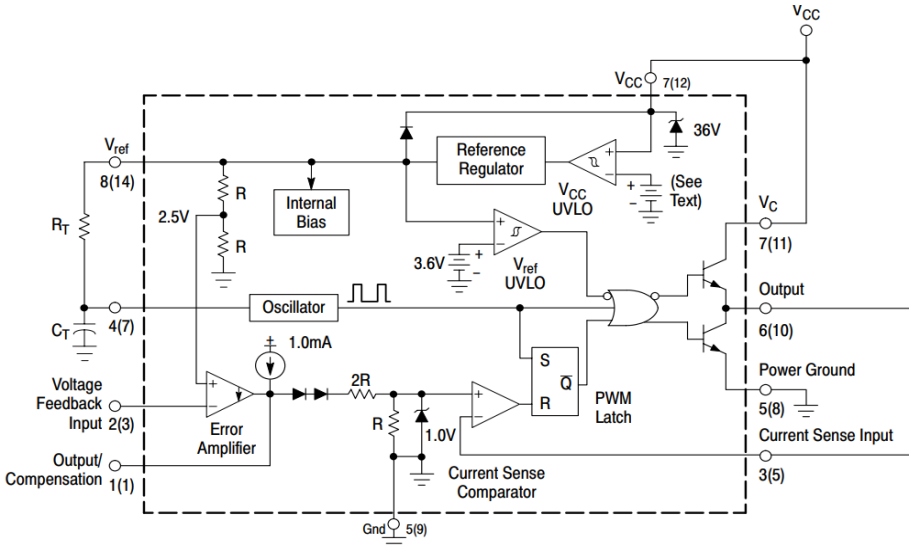

FIGURE 2. Block diagram of the PWM controller UC3842

With the *UC 3842 PWM* controller operating at *20 kHz,* the oscillation period is *50 μs*. The value of the capacitor C_4 can then be determined from the expression:

$$C_4 = \frac{\tau}{R} = \frac{50 \times 10^{-6}}{5 \times 10^{-3}} = 10 \ nF$$

Where: τ – is the time constant (*sec),* and *R* – is the error amplifier output resistance (ohms).

The values of the C_5 and C_7 filters, connected to the *UC 3842* PWM controller's voltage feedback input (input *2*) and current feedback input (input *3*), are selected during system setup. In this particular design, the filter value is *470 pF*.

The value of C_6, *100 nF*, connected to the reference voltage source output (pin 8), is selected according to the recommendations in the *UC 3842* datasheet.

Capacitors C_8 = *1 μF* and C_{10} = *0.33 μF* at the input and output of the *LM*7820 integrated voltage regulator are installed in accordance with the chip's data sheet.

The smoothing choke's inductance is found from the expression:

$$L_{CV} = \frac{U_{OUT} \times (1 - D)}{2 \times F \times \Delta I} = \frac{28 \times (1 - 0.453)}{2 \times 20 \times 10^{-3} \times 16} = 23.85 \ mk \ Gn,$$

Where L_{CV} – is the minimum critical inductance value; U_{OUT} – is the maximum output voltage on the batteries; D = *0.453* – is the duty cycle for *PWM* modulation, which is equal to the ratio of the minimum battery voltage of *24.5 V* to the maximum input voltage to the charge controller of *54 V; F = 20 kHz* – is the *PWM* modulation frequency; *I* – is the permissible current ripple level, assumed to be *10%* of the battery charging current, or *16 A*.

The calculated inductance value of *23.85 μH* is the minimum inductance value, and for reliable operation of the converter, it is necessary to use an inductance value twice that value. Therefore, we select the inductance value of *47 μH* for inductor L_1.

Capacitors C_9 = *10 mF* are connected in parallel with the batteries to filter out interference when switching the output power *MOSFET* transistors. The switching frequency of transistors VT_4, VT_5, and VT_6 is *20 kHz.*

The composite output stage, consisting of high-power *MOSFET* transistors, must switch a *160 A* pulsed battery charging current. The maximum voltage at the charge controller input is *95 V*. Therefore, p-type *MOSFET* transistors *DH100P70* with an allowable drain-source voltage of *100 V* and an allowable drain current of *75 A* were selected for the composite stage.

To determine the nominal value of capacitance C_9, we select an *LC* filter cutoff frequency half the switching frequency of the output transistors, equal to *10 kHz.*

Then the nominal value of capacitance C_9 is determined from the expression:

$$C_9 = \frac{1}{(2\pi F_{FCF})^2 \times L} = \frac{1}{(2 \times 3.14 \times 10 \times 10^3)^2 \times 47 \times 10^{-6}} = 5.39 \ \mu F,$$

Where $F_{FCF} = 10$ *kHz* – is the *LC* filter cutoff frequency; $L = 47$ μH – is the inductance of inductor L_1.

Using the *E24* series, we select a C_9 value of *5.1* μF.

The negative current and voltage feedback circuits are calculated as follows.

The negative current feedback signal is generated across resistor R_{23} and fed through resistor R_{15} to input *3* of the *UC3842 PWM* controller (see Fig. 2).

Input *3* of the *PWM* controller is connected to the inverting input of the *UC3842* current comparator, and a threshold voltage of *1 V* is generated at the non-inverting input of the current comparator, against which the negative current feedback signal is compared (see Fig. 2).

The current comparator's response threshold at input *3* will be limited by an internal threshold voltage of *1.0 V*. Therefore, with a total battery capacity of *800 A/h,* the maximum charging current will be *20%* of *800 A*, or *160 A*.

Then, the negative feedback resistance for the charging current, R_{23}, will be (see Fig. 1):

$$R_{OOC} = R_{23} = \frac{U_{TV.COMP.}}{I_{MAKC}} = \frac{1}{160} = 6{,}25 \times 10^{-3} \ Ом,$$

Where: R_{23} is the negative feedback resistance for the charging current; $U_{TVV.COMP.}$ is the threshold voltage of the *UC3842* current comparator, equal to *1 V*; I_{MAX} is the maximum battery charging current, equal to *160 A*.

For ease of charging current adjustment during system setup, the resistance value of R_{23} is selected to be twice as large as $R_{23} = 0.01$ *Ohm,* so that the calculated value of *6.25 x 10-3 Ohm* is at the midpoint of the potentiometer's value.

The voltage divider of the negative feedback circuit, R_4-R_5, is connected to the positive terminal of the batteries. For noise immunity, the current of the voltage divider of the negative feedback circuit, R_4-R_5, is selected to be at least *1 mA*. Then, with a minimum battery voltage of *24 V*, the maximum total resistance of the voltage divider, R_4-R_5, will be:

$$R_{4\text{-}5} = \frac{U_B}{I_{R4\text{-}5}} = \frac{24}{0.001} = 24 \ k \ Om,$$

Where U_B – is the minimum battery voltage; $IR_{4\text{-}5}$ – is the voltage divider value.

We select the voltage divider values $R_4 = 16$ *kOhm* and $R_5 = 5$ *k Om*.

The output voltage of the *UC3842 PWM* controller is *13.5 V* with a maximum permissible output current of *1 A*. The output signal of the *UC3842 PWM* controller is fed through resistor R_{21} to the base of the matching transistor VT_3.

Transistor VT_3 operates at a maximum collector voltage of 95 *V* and a collector current of *50 mA*.

VT_3 selects the *PBHV8115* transistor, which has the following characteristics:

- collector-emitter voltage of *150 V*;
- collector current of *1 A*;
- minimum current gain of *50* at a collector current of *50 mA* and *20 mA* at a collector current of *0.5 A*.

With a maximum collector current of transistor VT_3 of *50 mA,* the base current I_{BVT3} can be determined from the expression:

$$I_{BVT3} = \frac{I_{CVT3}}{\beta} = \frac{0.05}{50} = 0.001 \ A,$$

Where I_{BVT3} – is the base current of transistor VT_3; I_{CVT3} – is the collector current of transistor VT_3; β – is the minimum current gain.

A current of *1 mA* is sufficient to turn on transistor VT_3, but a boost mode with a base current reserve is required to generate the required edges when opening and closing the transistor.

To ensure reliable closing of transistor VT_3, resistor R_{21} with a nominal value of *120* ohms is installed between the base and emitter. The value of resistor R_{21} is specified during system setup.

Current flows to the base of transistor VT_3 from the *PWM* controller output through resistor R_{18}. Part of the current from the *PWM* controller output is subtracted from the base current of VT_3 and goes to ground through resistor R_{21}. With a voltage between the base and emitter of VT_3 of *0.8 V,* the current through resistor R_{21} can be determined from the expression:

$$I_{R21} = \frac{U_{BEVT3}}{R_{21}} = \frac{0.8}{120} = 0.0066 \ \ A,$$

Where U_{BEVT3} – is the voltage between the base and emitter of VT_3 in the on-state.

The saturation coefficient of transistor VT_3 is selected experimentally during system setup. In this particular case, taking into account the leakage current through resistor R_{21}, the base current of transistor VT_3 is set to 6 *mA*. Therefore, the value of resistor R_{18}, which limits the output current of the *PWM* controller to *6 mA*, is determined from the expression:

$$R_{18} = \frac{U_{OUT} - U_{BEVT3}}{I_{BVT3} + I_{R21}} = \frac{13.5 - 0.8}{0.006 + 0.0066} = 1007.9 \ \ kOhm,$$

Where U_{OUT} – is the *PWM* controller output voltage; U_{BEVT3} – is the voltage between the base and emitter of VT_3 in the on-state; I_{BVT3} – is the base current of transistor VT_3; I_{R21} – is the current of resistor R_{21}.

From the E24 series, we select resistor R_{18} =*1 k Om*.

Diode VD_2, connected between the base and emitter, is included for noise immunity of transistor VT_3.

The driver stage, built around transistors VT_1 and VT_2, must switch currents of up to *1 A* to recharge the input capacitances of output MOSFET transistors VT_4–VT_6.

Transistors VT_1 and VT_2 operate at a maximum collector voltage of *95 V* and a maximum current of *1 A.* Therefore, for the driver stage, we select a complementary pair of transistors VT_1 – *PBHV8215Z,* VT_2 – *PBHV9215Z.*

VT_1 and VT_2 have the following characteristics:

– Collector-emitter voltage of *150 V*;

– Collector current of *2 A*;

– Minimum current gain of *80* at a collector current of *1 A* and 55 at a collector current of *2 A*.

At a collector current of *1 A*, the base current of transistors VT_1 and VT_2 is found from the expression:

$$I_{BVT1\text{-}VT2} = \frac{I_{CVT1\text{-}VT2}}{\beta} = \frac{1}{55} = 0.018 \ \ A,$$

Where $I_{BVT1\text{-}VT2}$ – is the base current of transistors VT_1 and VT_2; $I_{CVT1\text{-}VT2}$ – is the collector current of transistors VT_1 and VT_2; β – is the minimum current gain.

Knowing the base current of transistors VT_1 *and* VT_2, we can determine the values of resistances R_{19} *and* R_{20}. The total resistance of R_{19} and R_{20} is determined from the expression:

$$R_{19\text{-}20} = \frac{U_{OUT.MIN}}{I_{BVT1\text{-}VT2}} = \frac{30}{0.018} = 1666.6 \ \ kOhm,$$

Where $R_{19\text{-}20}$ is the total resistance of resistors R_{19} and R_{20}; $U_{OUT.MIN}$ is the minimum voltage at the charge controller input, equal to *30 V*; $I_{BVT1\text{-}VT2}$ is the base current of transistors VT_1 and VT_2.

Therefore, each of the resistances R_{19} and R_{20} will be equal to *820 ohms*.

Resistance R_{22} *(51 ohms)* is designed to limit the current through transistors VT_1 *and* VT_2.

Diode VD_3 is designed to protect the output transistors from over voltages that occur when the current through inductor L_1 is interrupted.

Source E_3 in the circuit simulates the batteries. Resistance R_{24} is the load resistance of the charge controller.

Battery overcharge protection is controlled by a comparator built on operational amplifiers U_{2A} and U_{2B}. The reference voltage for the comparator is fed to the non-inverting input of operational amplifier U_{2A} from *1N5235* (VD_1). The value of the current-setting resistor R_6 of zener diode VD_1 is determined from the expression:

$$R_6 = \frac{E_{SV} - U_{SV}}{I_{SV}} = \frac{20 - 6.8}{0.01} = 1320\ ohm,$$

Where E_{SV} – is the comparator supply voltage of 20 *V*; U_{SV} – is the nominal stabilization voltage of the *1N5235* zener diode *(VD1)*; I_{SV} – is the stabilization current of the *1N5235 zener diode (VD1)*;

From the *E24* series, we select a resistor value of R_6 = *1.3 kOhm*.

The recharge voltage is fed to the comparator input from the battery output through voltage divider R_1-R_3 and resistor R_8 to the inverting input of operational amplifier U_{2A}. The voltage divider current is selected to be *1 mA* at a minimum battery voltage of *24 V*. Therefore, the total resistance of the voltage divider is:

$$R_{1\text{-}3} = \frac{U_{MIN}}{I_{R1\text{-}3}} = \frac{24}{0.001} = 24\ \ kOhm,$$

Where U_{MIN} is the minimum battery voltage; $I_{R1\text{-}3}$ is the voltage divider current.

Based on the total resistance of the voltage divider, we select the values of resistors R_1, R_3, and potentiometer R_2.

$$R_1 = 15\ k\ Om;\ R_2 = 3\ k\ Om;\ R_3 = 4{,}3\ kOhm.$$

The required hysteresis for noise immunity of the comparator is determined by the ratio of resistances R_7 and R_{11}.

The value of capacitor C_2 is selected during system setup for noise immunity.

In this circuit, operational amplifier U_{2B} is used as an inverting stage to match the input signal of the *PWM* controller. The ratio of negative feedback resistors R_{14} and R_{17} limits the gain of operational amplifier U_{2B} to *20*.

If charging the batteries causes the battery voltage to rise to *28 V,* battery overcharge control comparator U_2, via resistor R_{16} and optocoupler U_1, will generate a signal to stop generating the pulse-width modulated pulses, and the charge controller will stop sending the gate pulses to transistors VT_1–VT_6. This generates a signal to disconnect the rectifier from the charge controller input and a signal to activate the ballast resistors.

In addition to monitoring battery overcharge, a necessary battery protection function is monitoring for unacceptable battery discharge when the battery voltage reaches *24.5 V*.

The discharge voltage of *24.5 V* is controlled by the under-discharge control comparator (see Fig. 3).

The battery voltage signal is taken from the voltage divider R_3–R_4– R_5 and fed through resistor R_8 to the inverting input of operational amplifier U_{1A}. The hysteresis value for the comparator's noise immunity is set by the ratio of resistors R_7 – R_9. Voltage divider R_1 – R_2 in the comparator's mode simulation circuit simulates the battery voltage. The comparator's hysteresis is calculated so that when the battery voltage drops to *24.5 V*, the comparator signals the battery disconnection from the load. When the batteries charge to *27 V*, the load is reconnected. In the comparator's power section, resistor R_{17} simulates the winding of a power relay. Similar to the comparator for monitoring the unacceptable discharge of the battery, comparators for monitoring and protecting the wind turbine during a storm wind of *25 m/sec* and at an unacceptable high voltage at the output of the *3*-phase rectifier are constructed (see Fig. 4).

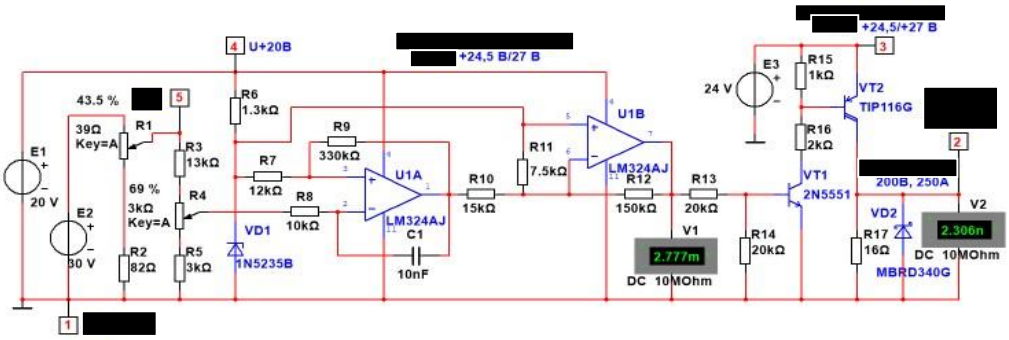

FIGURE 3. Comparator for protecting batteries from unacceptable discharge

When the emergency protection is triggered, the output of the *3*-phase rectifier is disconnected from the input of the charge controller and connected to the ballast resistors, which, in accordance with the value of the output voltage of the *3*-phase rectifier, connect the ballast resistors of the corresponding power.

CONCLUSIONS

1. Addressing alternative energy issues is a pressing issue today and creates new opportunities for wind energy development in Kyrgyzstan.
2. The relevance of developing alternative energy in Kyrgyzstan is also driven by the growing shortage of traditional energy sources.
3. An analysis of existing small-capacity wind turbines in Kyrgyzstan showed that wind energy development is promising and cost-effective.
4. Despite the fact that small-capacity vertical-axis wind turbines have lower wind energy utilization rates, the development of vertical-axis wind turbines in Kyrgyzstan is a promising direction due to their simple design and lower maintenance costs.

REFERENCES

1. Karatayev A.T., Isomidin kyzy K. Development of Technologies for the Use of Solar and Wind Power Plants. Bulletin of the Osh Technological University. 2023. No. 4. pp. 18-24.
2. Priority Areas of Energy Development in the Agro-Industrial Complex. A Collection of Articles Based on the Materials of the III All-Russian (National) Scientific and Practical Conference / 2019.
3. Current Issues in Energy in the Agro-Industrial Complex. Materials of the All-Russian Scientific and Practical Conference with International Participation / Blagoveshchensk, 2020.
4. Khakimov I.S., Miller M.V., Novikov V.F. Vertical-Axis Wind Power Plant for the Agro-Industrial Complex. Innovations in Agriculture. 2016. No. 5 (20). pp. 265-269.
5. Mokin B.I., Mokin A.B., Zhukov A.A. On the issue of choosing wind engines and electric generators of wind power stations. Bulletin of the Vinnytsia Polytechnic Institute. 2007. No. 6 (75). pp. 52-62.
6. Popova I.G., Kravtsov V.B., Kamelina E.S., Grebenyuk I.A. Study of the experience of using wind generatorsYoung researcher of the Don. 2021. No. 1 (28). pp. 2-9.
7. Kvitko A.V., Grigorash O.V., Popov A.Yu., Ivanovsky O.Ya., Tuaev A.S. Wind power stations. Krasnodar, 2017.
8. Goryunov O.A., Nazarova Yu.A. Prospects for Using Wind Turbines to Provide Power to Gas Industry Facilities in the Far North. Oil and Gas Territory. 2015. No. 12. pp. 146-150.
9. Kvitko AV, Azaryan AA. Design Features of Wind Power Stations. Krasnodar, 2022.
10. Afanasyeva NA, Dudnik VV, Gaponov VL. Study of the Operating Efficiency of a Small Wind Turbine under Yawing Conditions. Innovations in Agriculture. 2017. No. 2 (23). pp. 139-148.
11. Bugrova P.A., Goncharov N.A., Enbom A.I. Development of a Hybrid Battery Charge Controller for Powering Low-Power Consumers. Innovative, Information and Communication Technologies. 2019. No. 1. P. 378-382.
12. Kobersi I.S., Firov N.A., Sakhno D.A. Development of a charge-discharge controller for wind energy systems. Bulletin of SFedU. Engineering sciences. 2013. No. 2